Conference materials
UDC 538.915
DOI: https://doi.org/10.18721/JPM.183.202

Mechanism of resistive state switching in a non-filamentary memory device made of halide perovskite

A. Mahmoodpoor[1]✉, P.A. Alekseev[1,2], A.D. Furasova[1,3], S.V. Makarov[1,3]

[1] ITMO University, St. Petersburg, Russia;

[2] Ioffe Institute, St. Petersburg, Russia;

[3] Qingdao Innovation and Development Center, Harbin Engineering University, Shandong, China

✉ abolfazlmahmoodpoor@gmail.com

Abstract. In this study, we present a comprehensive numerical investigation of the modulation of the Schottky barrier in cesium lead bromide ($CsPbBr_3$) perovskite, focusing on the role of internal ionic charge carriers. We observe the pronounced hysteretic behavior in the current-voltage ($I–V$) characteristics of a metal-perovskite-metal configuration, where a 100 nm thick perovskite layer is sandwiched between chemically inert Schottky contacts. The inert nature of these contacts allows for the accumulation of mobile ions at the contact-perovskite interface without introducing secondary ion injections, thereby preventing any conducting filament formation. By implementing a one-dimensional drift-diffusion model, we simulate the dynamic evolution of mixed ionic-electronic charge carriers during $I–V$ measurements. Our findings reveal that resistive state switching (RSS) is predominantly influenced by ion accumulation at the interfaces, which effectively modulates the Schottky barrier and increases carrier tunnelling probability. Additionally, our analysis highlights the significance of polarized accumulated ions in achieving a more precise interpretation of experimental $I–V$ curves.

Keywords: semiconductor device simulation, numerical modelling, perovskite memristor, mobile ions in perovskite

Funding: This work was supported by the Russian Science Foundation (project № 24-62-00022).

Citation: Mahmoodpoor A., Alekseev P.A., Furasova A.D., Makarov S.V., Mechanism of resistive state switching in a non-filamentary memory device made of halide perovskite, St. Petersburg State Polytechnical University Journal. Physics and Mathematics. 18 (3.2) (2025) 16–23. DOI: https://doi.org/10.18721/JPM.183.202

Материалы конференции
УДК 538.915
DOI: https://doi.org/10.18721/JPM.183.202

Механизм переключения сопротивления в нефиламентном запоминающим устройстве из металлогалогенидного перовскита

А. Махмудпур[1]✉, П.А. Алексеев[1,2], А.Д. Фурасова[1,3], С.В. Макаров[1,3]

[1] Университет ИТМО, Санкт-Петербург, Россия;

[2] Физико-технический институт им. А.Ф. Иоффе РАН, Санкт-Петербург, Россия;

[3] Международный совместный исследовательский центр нанофотоники и метаматериалов, Харбинский инженерный университет, Шаньдун, Китай

✉ abolfazlmahmoodpoor@gmail.com

Аннотация. В данной работе представлено комплексное исследование модуляции барьера Шоттки в перовските $CsPbBr_3$, где уделяется особое внимание роли ионов как носителей заряда. Здесь наблюдается выраженное гистерезисное поведение вольт-амперных характеристик (ВАХ) для мемристоров с конфигурацией металл-перовскит-металл, где слой перовскита толщиной 100 нм расположен между химически инертными контактами Шоттки. Природа этих контактов позволяет накапливать подвижные ионы на границе контакт-перовскит без инжекции вторичных ионов, тем самым предотвращая образование проводящих нитей. Реализуя одномерную модель дрейфа-диффузии, удалось провести моделирование эволюции смешанных ионно-электронных носителей заряда во время измерений ВАХ. Результаты показали, что резистивное переключение состояний в основном зависит от накопления ионов на границе перовскит - контакт, что эффективно модулирует барьер Шоттки и увеличивает вероятность туннелирования носителей. Полученный результат подчеркивает значимость поляризованных накопленных ионов для более точной интерпретации экспериментальных характеристик перовскитных мемристоров.

Ключевые слова: моделирование полупроводниковых приборов, численное моделирование, перовскитный мемристор, подвижные ионы в перовските

Финансирование: Работа выполнена при поддержке Российского научного фонда (проект № 24-62-00022).

Ссылка при цитировании: Махмудпур А., Алексеев П.А., Фурасова А.Д., Макаров С.В. Механизм переключения сопротивления в нефиламентном запоминающим устройстве из металлогалогенидного перовскита // Научно-технические ведомости СПбГПУ. Физико-математические науки. 2025. Т. 18. № 3.2. С. 16–23. DOI: https://doi.org/10.18721/JPM.183.202

Introduction

Halide perovskites have emerged as a groundbreaking class of materials in the field of optoelectronics, particularly for applications in solar cells, light-emitting diodes, and photo detectors. The charge dynamics in halide perovskites are critical for understanding their performance in photovoltaic devices, as they involve processes of slow mobile ions and significantly change the current voltage (I–V) characteristics. The presence of mobile ions in halide perovskite devices can significantly hinder their performance, prompting researchers to seek methods to minimize ion redistribution [1–2]. Conversely, the mobility of ions within perovskite materials is not solely detrimental; it can also enable innovative applications, such as memristor devices [3] and photo detectors [4].

In the context of utilizing halide perovskite materials in memristor devices, the mechanism behind resistive state switching (RSS) can be attributed to three primary physical processes [5]. The first mechanism involves filament formation, where ionic filaments are generated either

through the injection of secondary ions from reactive metallic contacts such as silver or copper, or via the migration of halide vacancies. The second mechanism pertains to RSS that occurs through interface modulation. Lastly, the third mechanism is related to charge trapping and de-trapping in defect states, which influences the overall conductivity and switching behavior of the device. In the latter mechanism, RSS is attributed to the modulation of the interface between the perovskite layer and the charge transport layer. This process is particularly influenced by dipole formation and self-doping, which arise from the accumulation of ions at the interface [6–8]. In a separate study conducted by Guan and colleagues [9], the accumulation of ions at the perovskite/ITO interface was identified as a mechanism for RSS. They inferred that the buildup of negatively charged methylammonium vacancies at the perovskite/ITO interface, triggered by the application of a positive bias to the opposing electrode, leads to an enhancement of the Schottky barrier.

In this study, we aimed to clarify the mechanism of RSS in a single perovskite crystal by utilizing numerical calculations of drift-diffusion (DD) equations. Our analysis focused on the dynamics of electronic and ionic charge carriers within a $CsPbBr_3$ perovskite material sandwiched between two inert electrodes: a grounded boron-doped diamond (BDD) electrode and an indium tin oxide (ITO) electrode subjected to a positive bias. Our results indicate that filament formation does not occur; instead, we observed significant redistribution of internal mobile ions within the perovskite, leading to their accumulation at the perovskite/electrode interface. This ion accumulation critically alters the injection of charge carriers. By comparing our calculated I-V curve with experimental data, we demonstrated that, in addition to carrier tunneling from the electrodes, a reduction in the Schottky barrier is observed.

Materials and methods

To analyze the $I–V$ characteristics of the BDD-perovskite-ITO system, we utilized a one-dimensional DD model for ionic and electronic transport under transient conditions. The perovskite material positioned between two electrodes, is set at a thickness of 100 nm, reflecting experimental value. Due to the inability to inject or extract mobile ions from the electrodes, these ions tend to accumulate at the interface between the perovskite and the electrodes when a voltage is applied. This accumulation can lead to significant changes in the electric potential, potentially causing numerical instability in our simulations. To mitigate this issue, we implemented the well-established Scharfetter-Gummel (SG) method for discretizing current fluxes. While it is relatively straightforward to apply SG discretization to electronic carrier current density using the Boltzmann distribution [10], we adapted a modified version of SG discretization for ionic carriers, as suggested by Koprucki et al. [11].

System of equations

The system of transient DD equations will account for two types of carriers: ionic carrier with concentration of a for anions and c for cations, and electronics carrier with the concentrations of electrons n and holes p. The system of equations is:

$$\frac{\partial^2 V(x,t)}{\partial x^2} = -\frac{|q|}{\varepsilon\varepsilon_0}\left[p(x,t) - n(x,t) + c(x,t) - a(x,t) - N_A(x) + N_D(x) - N_{cat}(x) + N_{ani}(x)\right], \quad (1)$$

$$\frac{\partial n(x,t)}{\partial t} + \frac{1}{q}\frac{\partial j_n(x,t)}{\partial x} = U_n(x,t), \quad (2)$$

$$\frac{\partial p(x,t)}{\partial t} + \frac{1}{q}\frac{\partial j_p(x,t)}{\partial x} = U_p(x,t), \quad (3)$$

$$\frac{\partial a(x,t)}{\partial t} + \frac{1}{q}\frac{\partial j_a(x,t)}{\partial x} = 0, \quad (4)$$

$$\frac{\partial c(x,t)}{\partial t} + \frac{1}{q}\frac{\partial j_c(x,t)}{\partial x} = 0. \quad (5)$$

In Eq. (1), V is the electrical potential, ε_0 is the permittivity of free space and indicates the relative permittivity of the perovskite. The terms N_A and N_D are the concentrations of acceptors and donors' impurity, respectively. Additionally, we incorporate fixed concentrations of cations N_{cat} and anions N_{ani} to effectively model Schottky defects inside the perovskite [12]. Eqs. (2)–(5) demonstrate continuity equation for each charge carrier, where j_i and U_i, i = [n, p, a, c], are current density and net generation associated to each charge carrier. q is the elementary charge and it is negative for electrons and anions and positive for holes and cations. Current density for electron and holes can be written in the DD from as following:

$$j_n(x,t) = q\mu_n n(x,t)\frac{\partial V(x,t)}{\partial x} - qD_n\frac{\partial n(x,t)}{\partial x}, \tag{6}$$

$$j_p(x,t) = -q\mu_p p(x,t)\frac{\partial V(x,t)}{\partial x} - qD_p\frac{\partial p(x,t)}{\partial x}. \tag{7}$$

Conversely, it is appropriate to express the ionic DD current as follows:

$$j_a(x,t) = -q\mu_a a_{\lim} F\left[\eta_a(x,t)\right]\frac{\partial \varphi_a(x,t)}{\partial x}, \tag{8}$$

$$j_c(x,t) = q\mu_c c_{\lim} F\left[\eta_c(x,t)\right]\frac{\partial \varphi_c(x,t)}{\partial x}, \tag{9}$$

where F function is Blackmore distribution function and φ is quasi-Fermi level for ions. η_a and η_a are normalized electro-chemical potential of anions and cations, respectively, and connected to the quasi-Fermi levels as follows:

$$\eta_a(x,t) = \frac{|q|V(x,t) + \varphi_a(x,t)}{kT}, \tag{10}$$

$$\eta_c(x,t) = -\frac{|q|V(x,t) + \varphi_c(x,t)}{kT}. \tag{11}$$

Note that the Blackmore distribution function that describes hopping transport of ions between individual sites, is following:

$$F(\eta_i) = \frac{1}{e^{-\eta_i} + 1}. \tag{12}$$

In Eqs. (8) and (9), $a_{\lim}$ and $c_{\lim}$ represent limiting concentrations that limit the maximum accumulation of ionic carriers within the perovskite material. We implemented Schottky boundary conditions for electronic current fluxes, as will be described in the following sections, while applying zero flux conditions for ionic carriers. The main system of partial differential equations (PDEs), represented by Eqs. (1)–(5), was solved using the finite volume method. Additionally, we incorporated the WKB approximation based on method utilized by Kyounghoon et al. [10] to account for electron tunneling from the left (BDD), and hole tunneling from the right (ITO) contacts, respectively. Moreover, we considered the lowering of the Schottky barrier due to image force charges and dipole effects. The reduction in the Schottky barrier resulting from these influences can be described by the following equation [13]:

$$\Delta\Phi(t) = q\left[\beta\sqrt{\frac{q|E_m(t)|}{4\pi\varepsilon\varepsilon_0}} + \Gamma|E_m(t)|\right]. \tag{13}$$

In this equation, E_m represents the maximum of electric field at the surface of the electrodes.

Since there is no generation or recombination of mobile ions, the right-hand side of continuity equations for ions are zero. On the other hand, for electronic carriers we only considered trap assisted recombination. Therefore, $U_n = -R_n$ and $U_p = -R_p$, where R_n and R_p are recombination rate based on well-known Shockley-Read-Hall (SRH) model. As the boundary conditions we used Schottky boundary conditions and in addition to the Schottky barrier reduction we considered charge carrier tunneling.

Simulation geometry and parameters

The parameters used for our calculations are compiled in Table. Among the fitting parameters were the concentrations and mobilities of the ions, along with the parameters β and Γ from Eq. (13). Utilizing the simulation parameters specified in Table and applying SG discretization to solve the PDEs described by Eqs. (1)–(5), we initially established the equilibrium state for electronic carriers by presuming that ionic carriers had zero mobility. This equilibrium outcome was then used as a preliminary estimate for tackling the non-equilibrium situation, which began with ions distributed uniformly throughout the system.

Table

Simulation parameters for BDD-perovskite-ITO configuration

Parameter	Description	Value	Unit
T	Temperature	300	K
d	Perovskite thickness	100	nm
ε	Relative permittivity	12	1
χ	Electron affinity	–4.17	eV
IP	Ionization potential	–6.48	eV
N_D	Uniform donor concentration	0	cm^{-3}
N_A	Uniform acceptor concentration	$3 \cdot 10^8$	cm^{-3}
N_{CB}	eDOS of conduction band	$1 \cdot 10^{19}$	cm^{-3}
N_{VB}	eDOS of valance band	$1 \cdot 10^{19}$	cm^{-3}
μ_n	Electron mobility (Constant mobility model)	50	cm^2/Vs
μ_p	Hole mobility (Constant mobility model)	50	cm^2/Vs
N_{ani}	Uniform fixed anion concentration	$0.9 \cdot 10^{18}$	cm^{-3}
N_{cat}	Uniform fixed cation concentration	$1.3 \cdot 10^{19}$	cm^{-3}
μ_a	Anion mobility	$8.0 \cdot 10^{-9}$	cm^2/Vs
μ_c	Cation mobility	$4.0 \cdot 10^{-9}$	cm^2/Vs
a_{lim}	Limiting anion concentration	$1.41 \cdot 10^{22}$	cm^{-3}
c_{lim}	Limiting cation concentration	$4.67 \cdot 10^{21}$	cm^{-3}
Φ_n^l	BDD (left) contact Schottky barrier	0.63	eV
Φ_n^r	ITO (right) contact Schottky barrier	1.53	eV
β	Fraction of non-polarized ions	0.72	1
Γ	Thickness of accumulated polarized ions	1.25	nm
w^l	Maximum tunneling width from the ITO contact	10	nm
w^r	Maximum tunneling width from the BDD contact	10	nm
Area	Contacts area	$2.29 \cdot 10^{-11}$	cm^2

The device we simulated is depicted schematically in Fig. 1. This illustration shows a 100 nm thick layer of perovskite material positioned between a BDD and an ITO contact. A time-varying voltage is applied to the ITO, while the resulting calculated current is measured at the same contact.

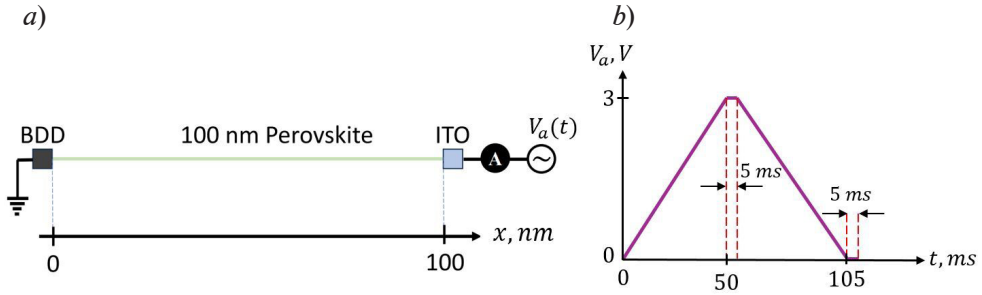

Fig. 1. Schematic of simulated device (*a*) and waveform of applied bias to the ITO (*b*)

We initialized the distribution of mobile ions to match that of the fixed ions. For solving the PDEs, we utilized a combination of the Gummel and Newton methods, leveraging the solution from the previous time step as the starting point for the current step. Given the nonlinear nature of the PDEs, we implemented a dynamic damping strategy as proposed by Amrein et al. [14].

Results and discussion

Utilizing the parameters detailed in Table, we calculated the $I-V$ curve for the BDD-Perovskite-ITO configuration, where the BDD is grounded and a positive triangular bias is applied to the ITO. The results of this calculation are depicted in Fig. 2. In panel (Fig. 2, *a*), we showcase six simulation cycles in green, juxtaposed with the experimental $I-V$ characteristics represented in orange. This comparison reveals a good correlation between the simulation results and the experimental data. The pronounced increase in current observed at 3 Volts corresponds to a 5 ms retention period at the peak of applied bias. Specifically, the ITO contact experiences a triangular pulse pattern, where each cycle consists of a voltage ramping up to 3 Volts and then back down to zero over a total duration of 110 ms. Each rise and fall within the cycle are symmetric, lasting 50 ms each. A pulse of one cycle is depicted in Fig. 1, *b*.

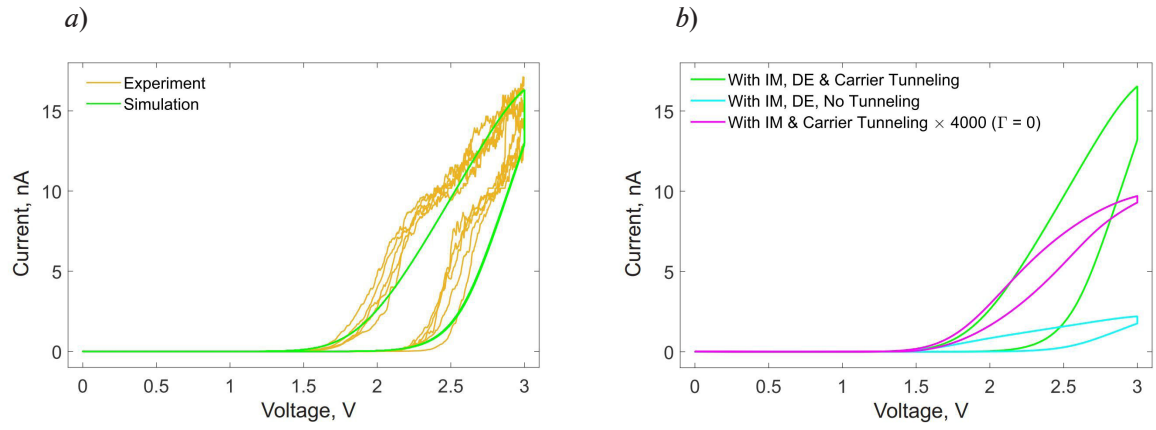

Fig. 2. Experimental (orange) and simulated (green) $I-V$ curves for 6 cycles of triangle potential pulse applied to the ITO (*a*); simulated $I-V$ curves illustrating the effects of varying carrier injection at the perovskite/contact interface (*b*). The green curve represents the scenario where both image charge force (IM) and dipole effects (DE) contribute to Schottky barrier lowering, along with carrier tunneling, the cyan curve depicts the $I-V$ characteristics without accounting for carrier tunneling but still considering Schottky barrier lowering due to IM and DE. The magenta curve illustrates the $I-V$ response solely influenced by IM and tunneling effects, excluding dipole effects in barrier lowering

In panel of Fig. 2, *b* we present three simulated $I-V$ curves corresponding to a single cycle of a triangular pulse, each reflecting different considerations regarding carrier injection from the contacts. The green curve mirrors the scenario depicted in panel (Fig. 2, *a*), where Schottky barrier lowering is accounted for through both image charge force (IM) and dipole effect (DE), alongside electron tunneling from BDD and hole tunneling from ITO. The cyan curve represents a similar calculation but omits the effects of carrier tunneling. A comparison of these two $I-V$ curves reveals that while their shapes are comparable, they differ significantly in amplitude; specifically, the firing potential in both forward and reverse bias scans remains largely consistent, with only amplitude variations. Conversely, the magenta curve illustrates the scenario where the dipole effect on barrier lowering is excluded, although the IM effect and carrier tunneling are still considered. This corresponds to the condition $\Gamma = 0$ in Eq. (13). To facilitate comparison with the other two curves, we have scaled this magenta curve by a factor of 4000. Notably, despite the three orders of magnitude difference in current amplitude, the firing potential in both forward and reverse bias scans remains unchanged in this case. This result diverges significantly from experimental observations, which indicate approximately a 0.8 Volt difference in firing potential between forward and backward scans. This analysis underscores the critical role of the dipole effect in Schottky barrier lowering at the perovskite/contact interface, particularly in scenarios involving significant ion accumulation.

Conclusion

In this study, we developed a one-dimensional ionic-electronic drift-diffusion model to analyze the $I-V$ characteristics of a perovskite material situated between two chemically inert contacts. Due to the disparities in Fermi levels between the contacts and the perovskite, both contacts function as Schottky barriers. Our numerical simulations accounted for carrier tunneling and the effects of Schottky barrier reduction. Tunneling emerges as a particularly promising mechanism, driven by the pronounced band bending near the contacts caused by ion accumulation. Additionally, the enhancement of the electric field at the electrode surfaces is crucial for elucidating the observed $I-V$ curves, as it contributes to the reduction of the Schottky barrier. Beyond the conventional image charge force that facilitates barrier reduction, our calculations reveal that the dipole moment induced by the accumulated mobile ions plays a significant role in further lowering the barrier height through a dipole effect. This insight enhances our ability to accurately model the $I-V$ characteristics. Furthermore, our findings indicate that filament formation is unlikely to occur solely through internal ion redistribution in the absence of external ion injection from reactive contacts. Instead, we propose that resistive state switching should be understood primarily because of interface modulation when external ions are not introduced. These findings mark a significant advancement in our understanding of resistive state switching mechanisms in non-filamentary perovskite memristors, providing valuable insights into their operational principles.

REFERENCES

1. **Yi H., Scheiner S., Tang X., et al.,** Suppression of hysteresis effects in organohalide perovskite solar cells, Advanced Materials Interfaces. 4 (11) (2017) 1700007.

2. **Satyaprasad S.P., Abdi-Jalebi M., Kamboj V.S., et al.,** A general approach for hysteresis-free, operationally stable metal halide perovskite field-effect transistors, Science advances. 6 (15) (2020) 4948.

3. **Yuhang L., Li F., Cui X., et al.,** Multiple B-site doping suppresses ion migration in halide perovskites, Science Advances. 11 (11) (2025) 7054.

4. **Bowen J., Chen X., Pan X., et al.,** Advances in Metal Halide Perovskite Memristors: A Review from a Co-Design Perspective, Advanced Science. 12 (2) (2025) 2409291.

5. **Yan X., Shen Z., Yuan S., et al.,** Ion migration mediated high Seebeck effect in halide perovskites and application in infrared detection, Chemical Engineering Journal. (477) (2023) 147168.

6. **Soumitra S., Raj K.Y., Adil Afroz M.,** Halide-perovskite-based memristor devices and their application in neuromorphic computing, Physical Review Applied. 18 (1) (2022) 017001.

7. **Congyang Z., Wang B., Li W., et al.,** Conversion of invisible metal-organic frameworks to luminescent perovskite nanocrystals for confidential information encryption and decryption, Nature communications. 8 (1) (2017) 1138.

8. **Sung-Il K., Lee Y., Park M.-H., et al.,** Dimensionality dependent plasticity in halide perovskite artificial synapses for neuromorphic computing, Advanced Electronic Materials. 5 (9) (2019) 1900008.

9. **Xinwei G., Hu W., Azimul Haque M., et al.,** Light-responsive ion-redistribution-induced resistive switching in hybrid perovskite Schottky junctions, Advanced Functional Materials. 28 (3) (2018) 1704665.

10. **Mahmoodpoor A., Makarov S.,** Numerical analysis of charge carriers injection in a light emitter or detector device based on a metal-semiconductor-metal structure, Photonics and Nanostructures-Fundamentals and Applications. (58) (2024) 101213.

11. **Koprucki T., Gärtner K.,** Discretization scheme for drift-diffusion equations with strong diffusion enhancement, Optical and Quantum Electronics. (47) (2013) 791–796.

12. **Calado P., Gelmetti I., Hilton B., et al.,** Driftfusion: an open source code for simulating ordered semiconductor devices with mixed ionic-electronic conducting materials in one dimension, Journal of Computational Electronics. (21) (2022) 960–991.

13. **Sze S. M., Li Y., Ng K.K.,** Physics of semiconductor devices, John wiley & sons. (2021).

14. **Amrein M., Wihler T.P.,** An adaptive Newton-method based on a dynamical systems approach, Communications in Nonlinear Science and Numerical Simulation. (19) (2014) 2958–2973.

THE AUTHORS

MAHMOODPOOR Abolfazl
abolfazlmahmoodpoor@gmail.com
ORCID: 0000-0002-7845-0592

FURASOVA Aleksandra D.
aleksandra.furasova@metalab.ifmo.ru
ORCID: 0000-0002-7277-5767

ALEKSEEV Prokhor A.
prokhor.alekseev@metalab.ifmo.ru
ORCID: 0000-0002-8143-4606

MAKAROV Sergey V.
svmakarov@itmo.ru
ORCID: 0000-0002-9257-6183

Received 19.08.2025. Approved after reviewing 25.09.2025. Accepted 25.09.2025.